Chinese Journal of Chemical Engineering 90 (2026) 146–156

Contents lists available at ScienceDirect

Chinese Journal of Chemical Engineering

journal homepage: www.elsevier.com/locate/CJChE

Full Length Article

Study on the decomposition mechanism of supercritical ethylene during ultra-high pressure polymerization process

Yao Chen [1, 2, 3, 4, #], Zhichen Zhang [1, 2, 3, #], Yunfeng Zhu [1, 2, 3], Haowen Chen [1, 2, 3], Yifan Song [1, 2, 3], Ruiyi Zhang [1, 2, 3], Xiaogang Shi [4], Bing Sun [1, 2, 3, *], Wei Xu [1, 2, 3, *]

[1] State Key Laboratory of Chemical Safety, Qingdao 266000, China
[2] SINOPEC Research Institute of Safety Engineering Co., Ltd. Qingdao 266000, China
[3] National Registration Center for Chemicals, Ministry of Emergency Management, Qingdao 266000, China
[4] College of Chemical Engineering and Environment, China University of Petroleum (Beijing), Beijing 102249, China

ARTICLE INFO

Article history:
Received 27 June 2025
Received in revised form
28 September 2025
Accepted 28 September 2025
Available online 27 November 2025

Keywords:
Ethylene decomposition
Ethylene polymerization
Low density polyethylene
ReaxFF molecular dynamics
Decomposition mechanism

ABSTRACT

In the production of low density polyethylene (LDPE), the presence of oxygen may induce the decomposition of supercritical ethylene, thereby affecting the stability of equipment operation and potentially leading to safety hazards. This study investigated the inducing and promoting effects of oxygen on the runaway decomposition of supercritical ethylene. The reaction mechanism of oxygen-induced supercritical ethylene was explored through ReaxFF molecular dynamics simulation, and the reaction network was systematically constructed. It was found that the minimum oxygen concentration required to initiate ethylene decomposition at 240 °C and 240 MPa was 0.0042% (mass). The coupling of oxygen and ethylene to form the intermediate $C_2H_xO\cdot$ promoted the cleavage of the C—C bond in ethylene. Under the condition of oxygen absence, ethylene mainly underwent polymerization reactions. As the oxygen concentration increased, unstable intermediates such as $C_2H_xO\cdot$ were generated, and the dominant reaction pathway of ethylene shifted from polymerization to decomposition. This study provided a theoretical basis for understanding the oxygen induced supercritical ethylene decomposition in low density polyethylene process.

1. Introduction

Low density polyethylene (LDPE) a thermoplastic resin characterized by a significant number of branched chains, which is polymerized by ethylene at 200–300 °C, 200–300 MPa. Due to its excellent transparency, insulation properties, corrosion resistance, and other characteristics, low density polyethylene is widely employed in the packaging and manufacturing of electrical insulation materials [1–3]. The global market value of LDPE is expected to exceed 170 billion dollars in 2029, with a large market scale and development prospects [4].

Ethylene polymerization is a highly exothermic reaction. Under conditions of 235 MPa and 150–300 °C, the specific heat capacity of ethylene is 2.51–2.85 $J\cdot(g\cdot°C)^{-1}$. If the heat released during polymerization is not completely dissipated, the polymerization of only 1% of ethylene can raise the temperature by 12–13 °C [5–7]. Such heat accumulation may subsequently trigger the decomposition of ethylene. The decomposition process of ethylene produces methane and hydrogen, accompanied by the release of heat [8], which is a significant thermal runaway process [9]. Thermal runaway leads to a sharp increase in temperature and pressure in the reaction system, leading to significant operational losses [10,11]. Albert *et al.* [12] clearly recorded the decomposition of ethylene polymerization caused by thermal runaway. The research showed that the initial pressure and temperature of ethylene polymerization were the key factors affecting ethylene decomposition. In the relevant reports on the cause statistics of unplanned shutdown of low density polyethylene process, ethylene decomposition is the direct cause of unplanned shutdown [13,14]. Oxygen can induce ethylene decomposition in ethylene polymerization, which is one of the main reasons for ethylene decomposition in industrial production [15].

As ethylene decomposition occurs exclusively under ultra-high pressure and temperature conditions, there is limited research in

* Corresponding authors.
E-mail addresses: sunb.qday@sinopec.com (B. Sun), xuw.qday@sinopec.com (W. Xu).
[#] These authors contributed equally to this work.

https://doi.org/10.1016/j.cjche.2025.09.031
1004-9541/

this area. Several studies have examined the mechanism of hydrocarbon decomposition using molecular simulations, which provide valuable insights for simulating ethylene decomposition. Zhou *et al.* [16] investigated the influence mechanism of ethanol on ethylene pyrolysis through numerical simulation, and the research indicated that oxygen in ethanol promoted the formation of C1 product. Song *et al.* [17] employed ReaxFF molecular dynamics simulations to investigate the mechanisms of high-temperature cracking and oxidation of ethylene and ethanol. Song *et al.* found that the polymerization of pure ethylene in the oxygen free environment mainly occurred with carbon chain growth and produced long-chain carbon. The addition of ethanol inhibited the production of long-chain carbon in ethylene polymerization, and the inhibition effect was more obvious with the increase of ethanol concentration. Oxygen in ethanol was finally released in the form of CO, CO_2 and H_2O. Martin and Akih Kumgeh [18] applied ReaxFF to the methane oxygen spontaneous combustion process at 20 MPa, and successfully captured the ignition delay time and main intermediate products using the NVT + NVE hybrid ensemble, verifying the reliability of ReaxFF in high-pressure combustion simulations. Chen *et al.* [19] simulated the pyrolysis of *n*-hexadecane under high pressures of 10, 30, 50, 70, and 90 MPa using ReaxFF molecular simulation. The calculated product data and kinetic data showed a high degree of agreement with experimental values. In the production of low density polyethylene, ethylene is in a supercritical state, which can be simply understood as increasing the pressure to promote intermolecular collisions. Although these studies can not directly reflect the decomposition mechanism of supercritical ethylene, they provide a reference for the molecular simulation of supercritical ethylene decomposition.

However, due to the high requirements of the ultra-high pressure ethylene reaction runaway testing device, the publicly available ultra-high pressure research is limited, and the influence of trace oxygen on ethylene in the low density polyethylene system has not been studied [20]. In addition, the lack of experimental data has hindered the exploration of the ethylene decomposition mechanism in the low density polyethylene system.

Based on the above problems, this work investigated the decomposition behavior of supercritical ethylene under oxygen-containing conditions through the ultra-high pressure ethylene decomposition runaway test characterization platform. The effects of oxygen concentration and ethylene density on the decomposition temperature, decomposition pressure and decomposition products of supercritical ethylene were investigated. The evolution mechanism network of oxygen concentration induced supercritical ethylene decomposition was constructed by ReaxFF simulation. This article aims to develop a comprehensive understanding of oxygen-induced decomposition of supercritical ethylene through experimental and simulation studies.

2. Experimental and Simulation

2.1. Materials

The experiment used 99.999% ethylene as raw material to explore the evolution mechanism of ethylene decomposition. The air cylinders contained 20.9% oxygen to provide oxygen environment for the system.

2.2. Ethylene decomposition test device and operation process

Before ethylene entered the reactor, it needed to be liquefied in the ethylene raw material tank under the set condition of −10 °C and 4 MPa. The liquefied ethylene was delivered to the reactor through the liquid pump once the reactor temperature reached the set temperature. Due to the high temperature in the reactor, the liquefied ethylene underwent phase change expansion after entering the reactor, causing the pressure in the reactor to rise. The set pressure of the reaction system was reached by continuously adding ethylene to the reactor. Ethylene in the reactor was initiated by tungsten wire, and the temperature and pressure changes during ethylene decomposition were collected through the DCS control system. The ethylene decomposition products were collected for further research and analysis. The ethylene decomposition device was shown in Fig. 1.

2.3. Experiments for the decomposition of ethylene

The experimental conditions of ethylene decomposition were 240 °C and 240 MPa, which were closer to actual production. The effect of oxygen concentration on the evolution mechanism of ethylene decomposition was investigated. The oxygen concentration range was 0.001%−1.0% (mass). The decomposition condition of ethylene was named O*x*, where *x* represented oxygen concentration.

The research on ethylene decomposition mainly included maximum decomposition pressure (P_{max}) and maximum decomposition temperature (T_{max}). The ethylene decomposition curve was divided into three stages: energy accumulation, violent decomposition, and stability after decomposition, to reflect the evolution of ethylene decomposition under different oxygen concentrations.

2.4. Characterization

The composition and content of the gas generated after ethylene decomposition were characterized by gas chromatography-mass spectrometry (GC-MS). GC-MS is composed with two Agilent 7890BGC instruments equipped with FID and TCD detectors and MolsieveSA, HayeSep Q, PoraBOUND U, and HP-AL/S column [21].

The surface morphology of derived carbon powder was observed by S-4800 scanning electron microscopy (SEM) (Hitachi, Ltd., Japan) combined with energy dispersive X-ray spectroscopy (EDS) [22,23].

The X-ray diffraction (XRD) analysis was performed on an X'Pert Pro MPD X-ray diff; ractometer (PANalytical B.V.) equipped with a Cu K_α radiation. The scan rate was set to $10(^\circ)\cdot min^{-1}$ with a step size(2θ) of 0.017°, and the scan range was between 5° and 75°. XRD provided the stacking order degree of carbon powder and lattice stacking parameters, such as interlayer spacing d_{002}, stacking height L_C and stacking layer number N. The stacking height L_C was calculated according to the Scherrer formula and the interlayer spacing d_{002} was calculated by Bragg formula. The stacking layer number N was calculated by the formula: $N = (L_C/d_{002}) + 1$ [24–26].

Raman spectra were tested by using a Labram 10 Raman spectrometer with a He-Ne laser as excitation source and were performed with the Gaussian curve-fitting method as a reasonable method to judge the structural defect and ideal graphite degree of the derived carbon powder. Five Raman bands were divided according to the Gaussian curve-fitting method: 1580 cm^{-1} of G band represented ideal graphitic lattice (E_{2g}-symmetry); 1350 cm^{-1} of D1 band represented disordered graphitic lattice (graphene layer edges, A_{1g} symmetry); 1620 cm^{-1} of D2 band represented disordered graphitic lattice (surface graphene layers, E_{2g}-symmetry); 1500 cm^{-1} of D3 band represented amorphous carbon (Gaussian line shape); 1200 cm^{-1} of D4 band represented disordered graphitic lattice (A_{1g} symmetry), polyenes, ionic impurities [27].

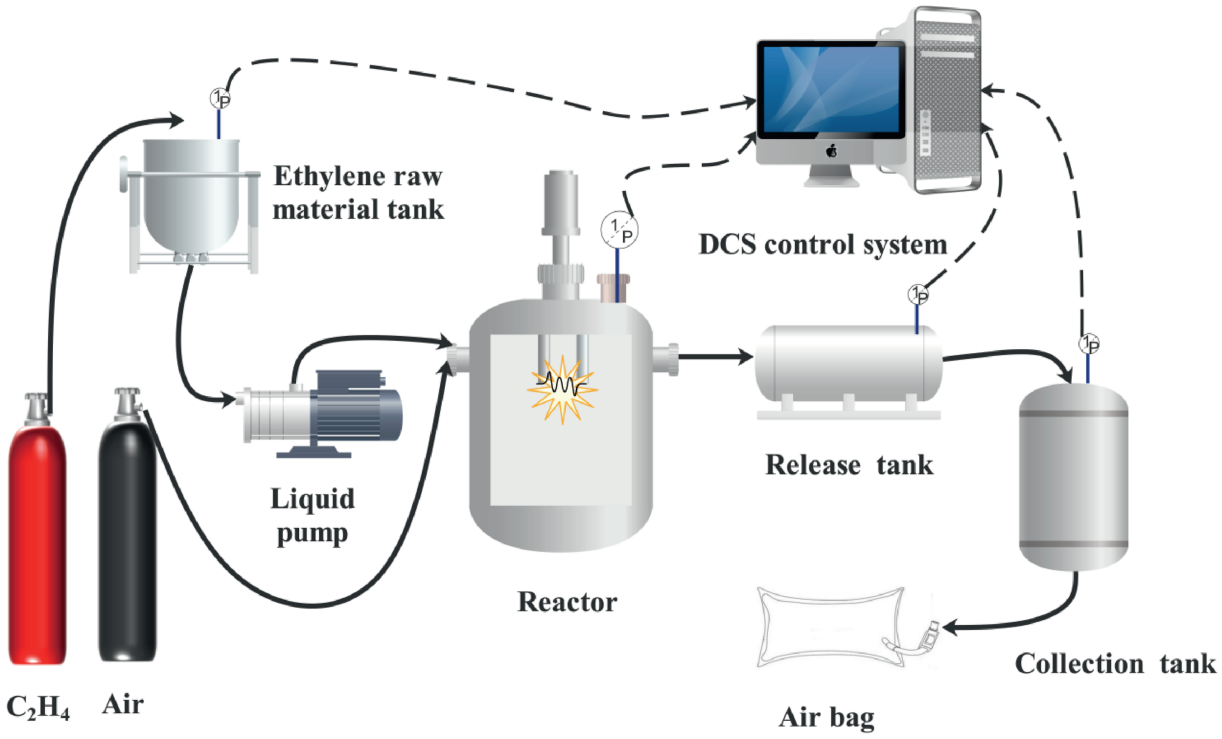

Fig. 1. The decomposition device of ethylene.

Fourier transform infrared spectra (FTIR) of the decomposition carbon powder were measured by using an FTIR spectrometer (NEXUS FT-IR, Nicolet), the resolution for operation was 2 cm^{-1}, while the scan range was from 400 to 4000 cm^{-1}. The FTIR spectra was mainly used for determining the functional group structure after the decomposition of ethylene [28].

2.5. Construction of three-dimensional models

Materials Studio software was used to model the oxygen induced ethylene decomposition system. Four oxygen systems with the number of oxygen molecules 0, 20, 40 and 60 were constructed, as shown in Fig. 2, and each system contained 60 ethylene molecules. Periodic boundary conditions were applied in all directions to minimize surface effects and to approximate bulk-phase behavior with a finite number of molecules. Under supercritical conditions, where intermolecular interactions are mainly short-ranged, periodic boundary conditions ensure that each molecule experiences an environment representative of an effectively infinite system. This approach enables a reasonable representation of the supercritical ethylene system at the selected simulation scale. The initial density of the system was set to 0.478 $g \cdot cm^{-3}$, corresponding to the experimentally measured density of ethylene at 200 MPa and 200 °C.

2.6. Reaction force field

Reaction Force Field (ReaxFF) is a force field based on the concept of bond order. By dynamically calculating the distance between atoms to update the bond order in real time, the breaking and formation of chemical bonds during chemical reactions can be precisely described, and the bonding and non-bonding interactions in complex systems can be captured. The parameters of ReaxFF mainly come from quantum chemistry calculation data, combining the precision of quantum chemistry with the computational efficiency of molecular dynamics, and are suitable for the

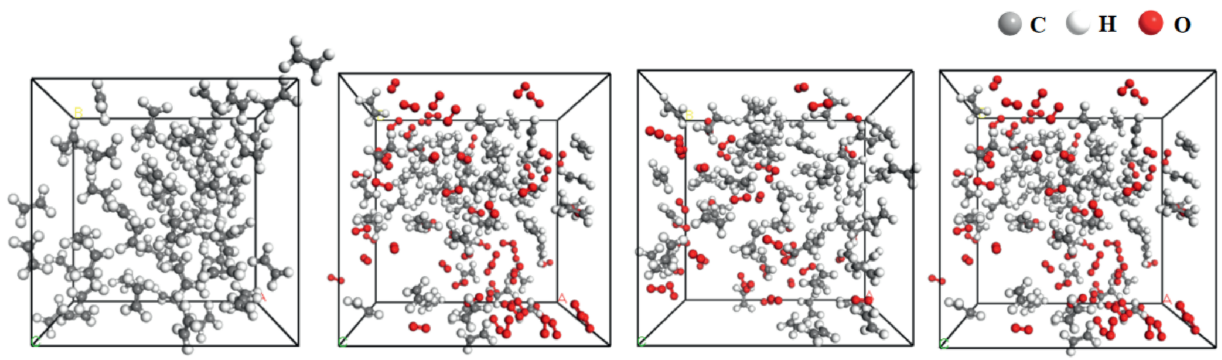

Fig. 2. Ethylene decomposition system: (a) no oxygen; (b) 20 oxygen molecules; (c) 40 oxygen molecules and (d) 60 oxygen molecules.

simulation of large-scale systems. Its application fields cover the research on complex reaction mechanisms such as pyrolysis, oxidation, catalytic reactions, and combustion processes [29,30].

$$E_{system} = E_{bond} + E_{over} + E_{under} + E_{val} + E_{pen} + E_{tors} + E_{conj} + E_{vdW} + E_{Coul} \quad (1)$$

where E_{bond} is the bond energy, E_{over} is the over coordination, E_{under} is the under coordination, E_{val} is the valence angle energy, E_{pen} is the penalty energy, E_{tors} is the torsion angle energy, E_{conj} is the conjugation effects on molecular energy, E_{vdW} is the van der Waals interaction, and E_{Coul} is the Coulomb interactions.

2.7. Computational details

The simulation of this study was realized by LAMMPS software and the reaction force field was CHO-2016 [31]. Ethylene decomposition simulation was carried out under NVT ensemble, and Berendsen thermostat was used for temperature control. Due to the slow decomposition of ethylene at low temperature, a lot of computing resources were required. Increasing the reaction temperature could accelerate the process of ethylene decomposition reaction without changing the ethylene decomposition mechanism. After testing various temperature conditions, the simulation temperature was selected as 4000 K based on the accuracy and efficiency of the simulation. The simulation time step was 0.1 fs, and the total simulation time was 200 ps.

3. Results and Discussion

3.1. The decomposition of ethylene

3.1.1. The effect of oxygen concentration on ethylene decomposition

Fig. 3 reflected the effect of oxygen concentration on the maximum pressure (P_{max}) and the maximum temperature (T_{max}) of ethylene decomposition at 240 °C and 240 MPa. It is found that both P_{max} and T_{max} showed upward trends with the increase of oxygen concentration in the system. When the oxygen concentration was 1.0% (mass), the P_{max} of ethylene decomposition reached 1107 MPa and the T_{max} of decomposition was up to 1236 °C. As the oxygen concentration was 0.0042%, the P_{max} and T_{max} after ethylene decomposition were 532 MPa and 553 °C, respectively. The oxygen concentration of 0.0042% was the lower

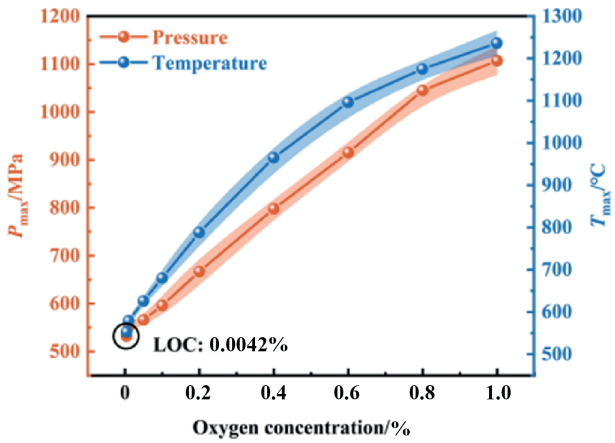

Fig. 3. P_{max} and T_{max} changing trends for ethylene decomposition with the increase of oxygen concentration at 240 °C and 240 MPa.

limit of ethylene decomposition under the reaction condition of 240 MPa and 240 °C. Oxygen free radical accelerated ethylene polymerization to produce more hot spots, leading to proceeding ethylene decomposition. As the oxygen concentration increased, the ethylene decomposition produced a greater gas volume expansion, a faster gas expansion rate, and a more intense energy release. The explosion wave generated by ethylene decomposition reached extremely high pressure in an instant, which greatly aggravated the explosion effect.

The density of ethylene had an apparent influence on ethylene decomposition, the variation curves of P_{max} and T_{max} with ethylene density were exhibited in Fig. 4. It is found that the P_{max} and T_{max} of ethylene decomposition increased with the rise of ethylene density. While the oxygen concentration was 0.01%, the density of 0.3 $g \cdot m^{-3}$ possessed the lowest P_{max} and T_{max} of 307 MPa and 387 °C, and the density of 0.55 $g \cdot m^{-3}$ had the highest P_{max} and T_{max} of 532 MPa and 579 °C. The increase in the initial density of ethylene reduced molecular spacing, thereby increasing the probability of molecular collisions, improving heat and mass transfer efficiency between molecules, and ultimately accelerating the ethylene decomposition reaction. In addition, the rising initial density enhanced reactants concentration, and the decomposition of ethylene generated more gas and heat, resulting in a higher rise in pressure and temperature.

3.1.2. Research on decomposition behavior of ethylene

The decomposition behavior primarily focused on the changing trends of decomposition pressure and temperature, as well as the time points during the decomposition evolution process. Fig. 5 demonstrated the pressure changing curve of ethylene decomposition evolution process at 240–240 MPa with the oxygen concentration of 0.1%. According to the evolution characteristics of pressure in the process of ethylene decomposition, the ethylene decomposition process was split into three stages: energy accumulation, instantaneous pressure rise and pressure stabilization. Energy accumulation stage referred to the stage from the start of ignition until the sharp change of ethylene decomposition pressure, and this period was represented by T_1. In instantaneous pressure rise stage, the ethylene decomposition pressure rose sharply and reached the maximum pressure, and the time for this stage was T_2. The final stage was pressure stabilization, and the ethylene decomposition pressure decreased from the highest point to stable, and the time taken was represented by T_3. Moreover, t_{Px} and t_{Tx} were the time corresponding to pressure and temperature change respectively.

Table 1 listed the time nodes of ethylene decomposition evolution process at 240–240 MPa. The results showed that the increase of oxygen concentration reduced the time of ethylene decomposition energy accumulation, and the ethylene decomposition evolution process was more rapid. While the oxygen concentration increased from 0.0042% to 1.0%, the t_{P1} decreased from 14 s to 2 s, and the t_{P2} lowered from 8 s to 0.6 s. Oxygen free radicals produced by oxygen decomposition provided a large number of active sites for ethylene reaction, which aggravated the ethylene decomposition behavior and worsened the degree of ethylene decomposition.

In addition, as the oxygen concentration was relatively low, the ethylene decomposition temperature changed first, and the decomposition pressure had a lag variation. The lag variation of pressure gradually weakened with the increase of oxygen concentration. t_{P1} and t_{T1} were 14 s and 9 s respectively under the 0.0042% of oxygen concentration, and while the oxygen concentration was increased to 1.0%, t_{P1} and t_{T1} were both 2 s. This is because while the oxygen concentration was low, ethylene first underwent a short polymerization reaction. As the polymerization heat reached the critical point of ethylene decomposition, a mass of gases were generated from ethylene decomposition, leading to

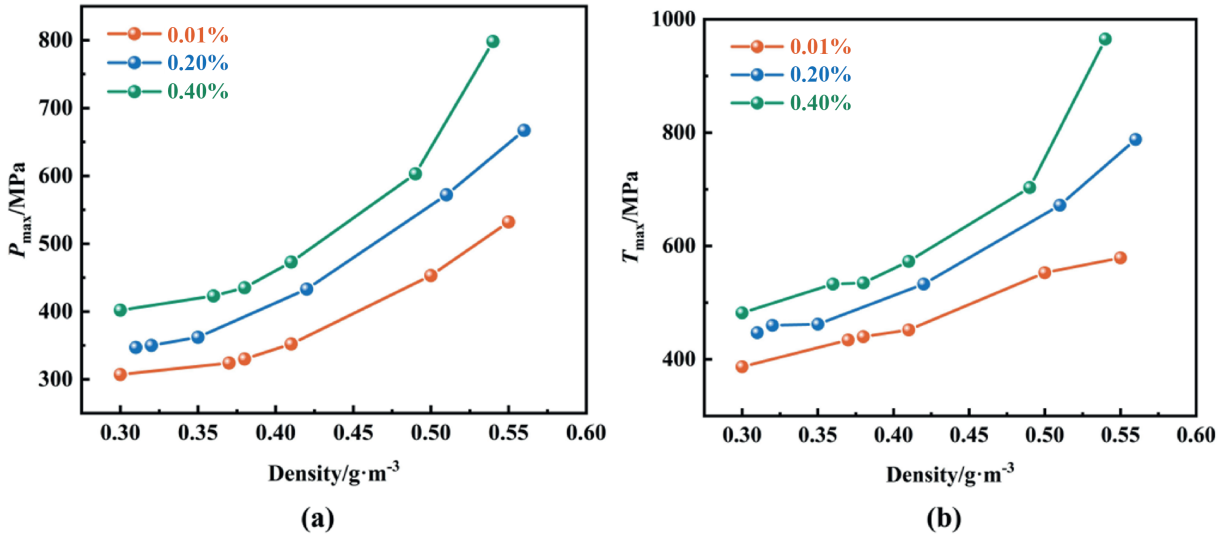

Fig. 4. P_{max} and T_{max} changing trends for ethylene decomposition with the increase of oxygen concentration and ethylene density: (a) P_{max}; (b) T_{max}.

the pressure to rise. The increase of oxygen concentration intensified the reaction activity of ethylene. Ethylene directly reacted with a significant number of oxygen free radicals to decompose, generating a substantial amount of heat and gas simultaneously, indicating that the decomposition temperature and pressure of ethylene tend to change concurrently.

3.2. Analysis of ethylene decomposition products

3.2.1. Analysis of gas products after ethylene decomposition

The relative content of gas produced by ethylene decomposition under different oxygen concentrations at 240–240 MPa was displayed in Fig. 6. The gaseous products of ethylene decomposition primarily consisted of methane, hydrogen, and small amounts of carbon monoxide and carbon dioxide. The results demonstrated that the relative contents of methane, carbon

Table 1
The decomposition time nodes for ethylene decomposition at 240–240 MPa.

C_{O_2}/%	t_{P1}/s	t_{T1}/s	t_{P2}/s	t_{T2}/s
0.0042	14	9	8	5
0.01	13	8	8	5
0.05	13	7	8	5
0.1	11	6	6	3
0.2	8	6	6	3
0.4	4	4	3	2
0.6	3	3	2	2
0.8	3	2	1	1
1.0	2	2	0.6	0.62

Note: C_{O_2}, Oxygen concentration; t_{P1}, Energy accumulation time of decomposition pressure; t_{T1}, Energy accumulation time of decomposition temperature; t_{P2}, Instantaneous pressure rise time of decomposition pressure; t_{T2}, Instantaneous temperature rise time of decomposition temperature.

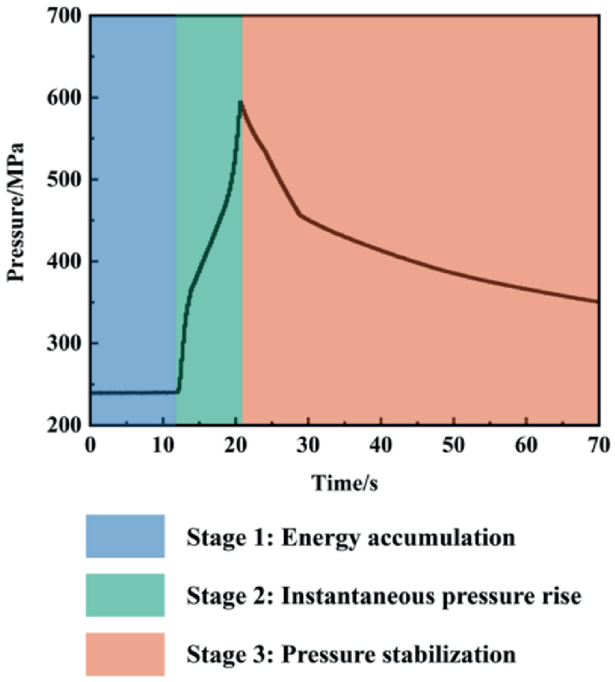

Fig. 5. The pressure changing curves of ethylene decomposition at 240–240 MPa with oxygen concentration of 0.1%.

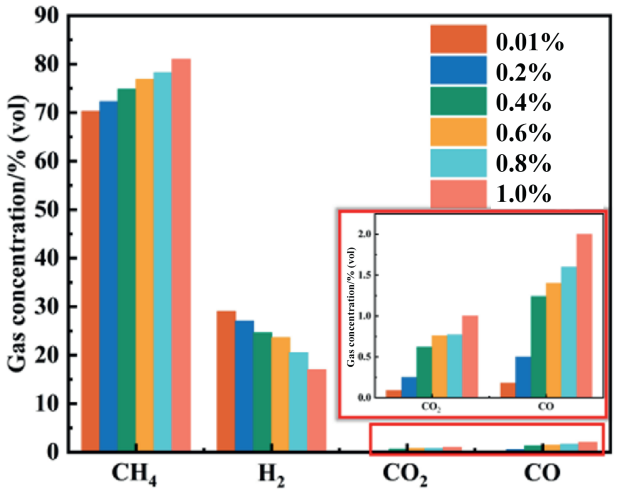

Fig. 6. The gas product composition of ethylene decomposition at 240–240 MPa.

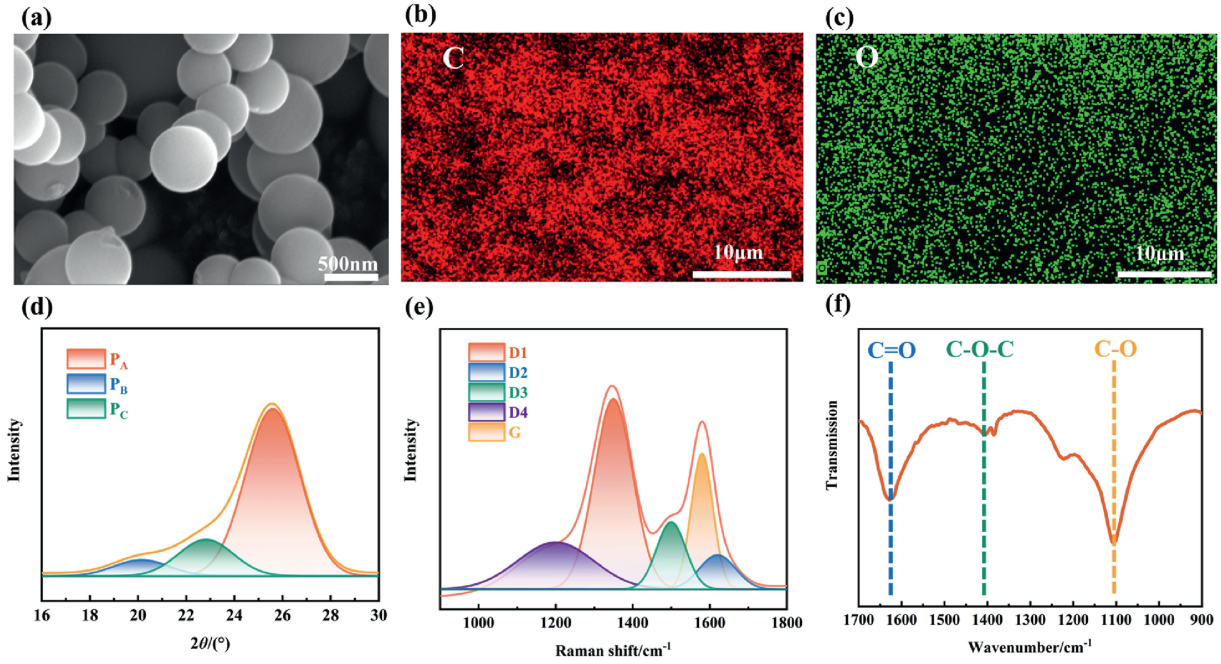

Fig. 7. Structural feature characterization analysis of generated carbon produced under 240–240 MPa and the oxygen concentration of 0.1%: (a) SEM; (b) EDS mapping of C; (c) EDS mapping of O; (d) XRD; (e) Raman and (f) FTIR.

monoxide, and carbon dioxide increased with increasing oxygen concentration. When the oxygen concentration was 1.0%, the maximum relative content of methane was 80.92%, and the relative contents of carbon monoxide and carbon dioxide were also highest, though each remained below 2%. The elevated oxygen concentration enhanced ethylene decomposition, increasing the frequency of C—C bond cleavage, which led to an increase in methane, carbon monoxide, and carbon dioxide. The relative content of hydrogen decreased with increasing oxygen concentration, and the peak relative hydrogen content of 29.03% occurred at the oxygen concentration of 0.01%. The primary reason for the reduction of hydrogen was that oxygen reacted with hydrogen to form water.

3.2.2. Characteristics analysis of solid products after ethylene decomposition

Fig. 7 illustrated the morphology and structural characterization of carbon powder produced by ethylene decomposition at 240 °C, 240 MPa and oxygen concentration of 0.1%. Fig. 7 (a) clearly demonstrated that the carbon powder had a microspherical structure with a smooth surface and high sphericity. Fig. 7 (b) and (c) illustrated the uniform distribution of carbon (C) and oxygen (O) elements on the carbon powder, as revealed by EDS mapping. The XRD fitting curves of the carbon powder were presented in Fig. 7 (d), displaying a distinct 2θ peak at approximately 26° corresponding to crystalline carbon, along with two additional peaks indicative of amorphous carbon. The Raman fitting curves shown

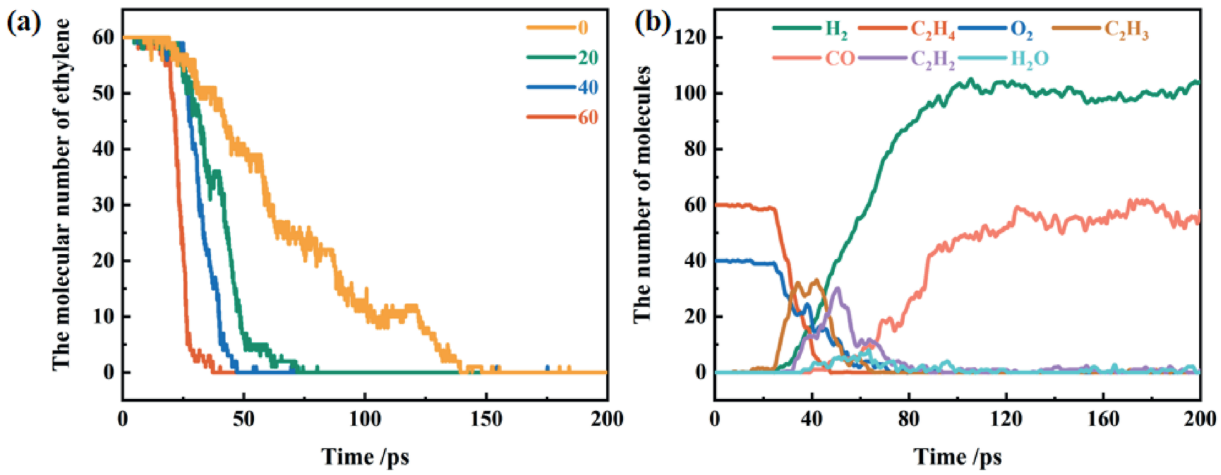

Fig. 8. (a) Influence curve of oxygen concentration on ethylene decomposition rate; (b) the change curves of reactants and products during ethylene decomposition under the oxygen molecular number of 40.

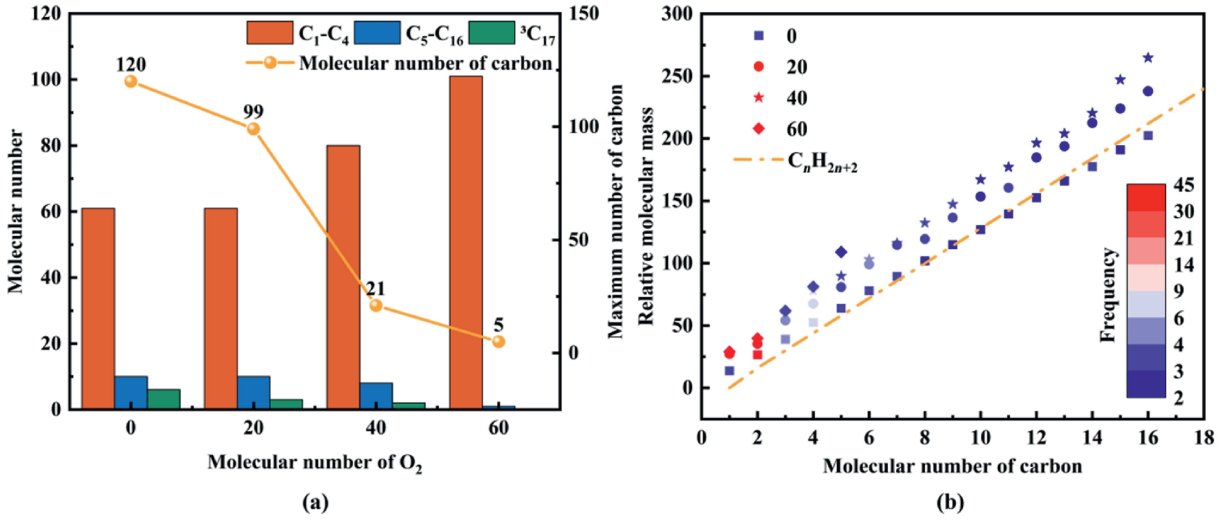

Fig. 9. Distribution of carbonaceous products in ethylene decomposition: (a) proportion of products and maximum carbon content; (b) molecular weight and occurrence frequency of products.

in Fig. 7 (e) reflected the degree of graphitization and disorder in the carbon powder lattice. The results indicate that the structural defects in decomposed carbon powder primarily occur at the edges of the graphene layers. The analysis results of FTIR in Fig. 7 (f) displayed distinct C═O and C—O peaks, indicating that the primary cause of the structural defects in carbon powder was the

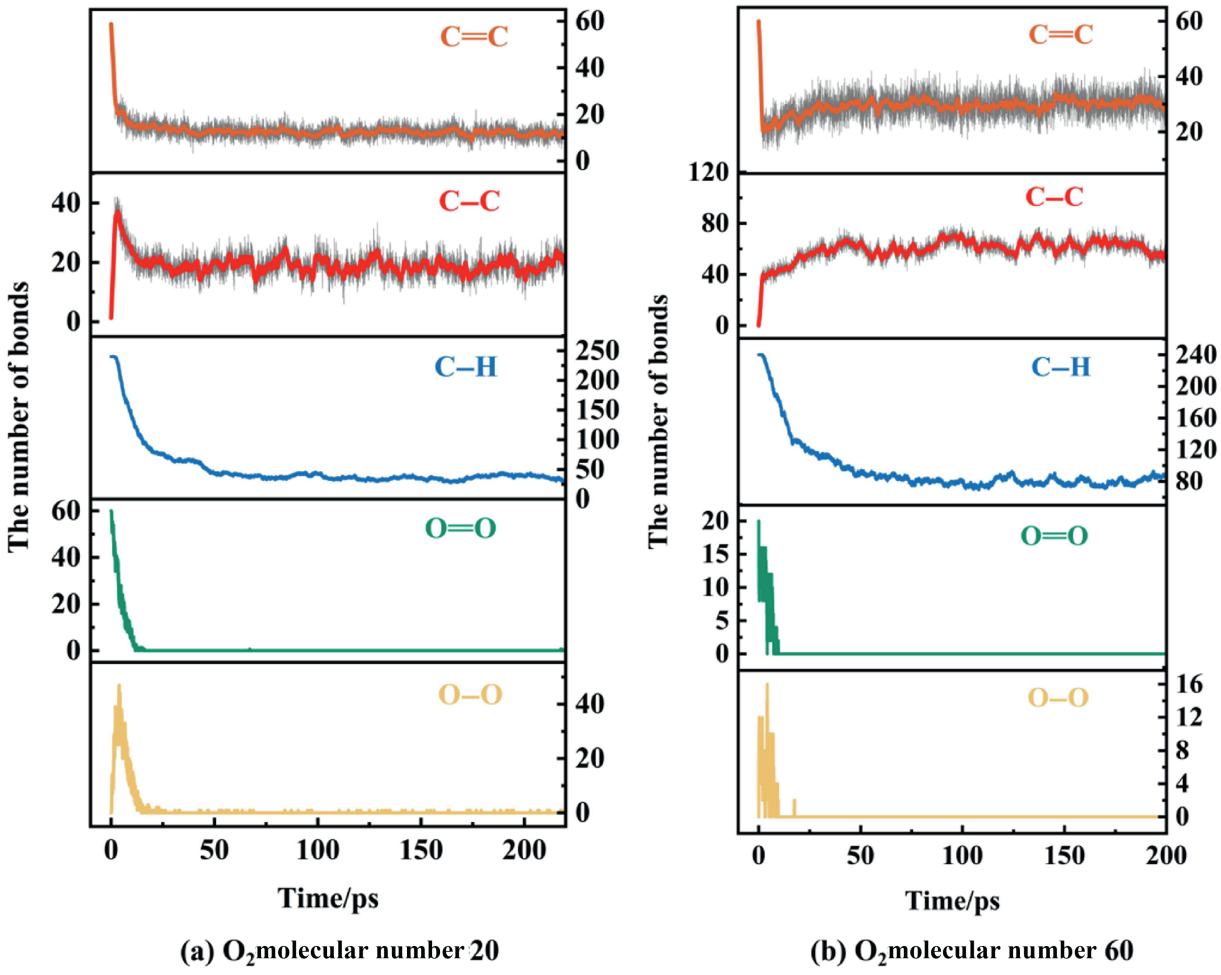

Fig. 10. Variation curves of chemical bond number during ethylene decomposition process under different oxygen concentrations: .

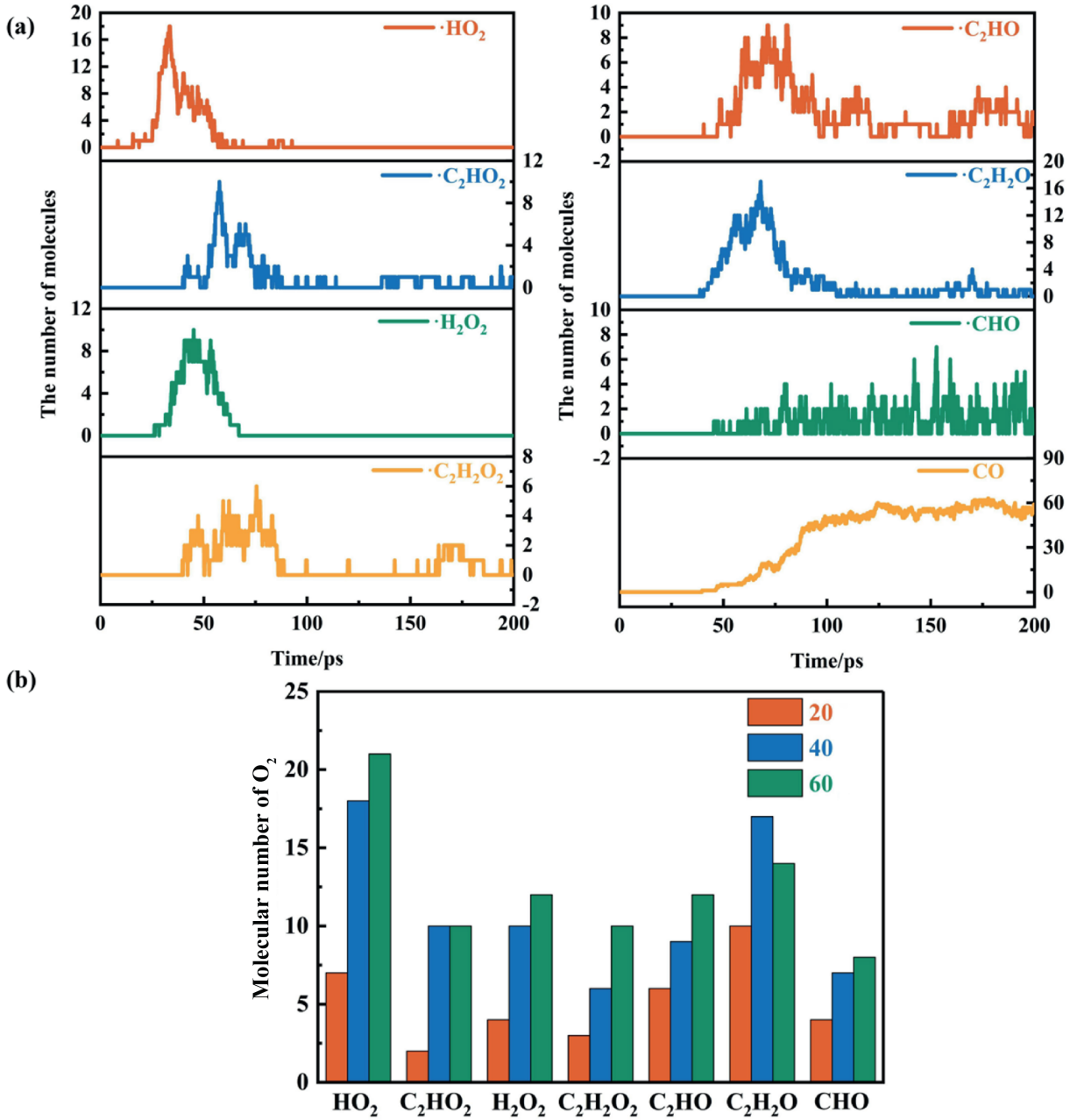

Fig. 11. (a) The time-dependent curves of key oxygen-containing groups and products in ethylene decomposition under the condition of oxygen molecular number of 60, and (b) impact on oxygen concentration on key oxygen-containing groups.

stretching vibrations of C—O and C═O bonds, generated by the interaction of ethylene and oxygen. The oxygen-containing groups exhibited significant steric hindrance, leading to uneven stacking of the lattice layers and defects in the pore structure.

3.3. Mechanism of ethylene decomposition

3.3.1. Product distribution

Fig. 8 illustrated the impact of oxygen concentration on the ethylene decomposition rate and the temporal variations of reactants and products during the decomposition. It was evident that an increase in oxygen concentration accelerated the ethylene decomposition rate in Fig. 8 (a). In the absence of oxygen in the simulated system, ethylene decomposed completely at 139 ps. While the number of oxygen molecules in the system was 60, corresponding to a molar ratio of 1:1 for ethylene to oxygen, ethylene decomposed completely at 37 ps. Fig. 8 (b) showed the changes of reactants and products with time during ethylene reaction in the system of oxygen molecular number 60. The time of ethylene consumption was the time of C_2H_3 radical generation. While the number of C_2H_3 radical reached the peak, C_2H_2 radical began to produce. In addition, the results showed that the dehydrogenation rate of ethylene was faster than oxygen to produce oxygen free radicals. This indicated that the dehydrogenation of ethylene mainly occurred in the initial stage of ethylene reaction and less oxygen free radicals directly attacked ethylene to decarburize.

By analyzing the carbon content of ethylene reaction products, the pathway of ethylene consumption could be determined. The variation of carbon containing products from ethylene reaction

with oxygen concentration was reflected in Fig. 9 (a). The maximum carbon content in the ethylene reaction products decreased with increasing oxygen concentration, while the proportion of gas products (C_1–C_4) rose. In the oxygen-free system, the maximum carbon content in the ethylene reaction products was 120, indicating that ethylene in the system underwent polymerization to produce LDPE with a degree of polymerization of 120. In the system with 60 oxygen molecules, the maximum carbon content in the product was 5, and the proportion of products with fewer than 5 carbon atoms accounted for more than 99%. This indicated that ethylene directly reacted with oxygen to decompose into small molecular products. Fig. 9 (b) showed that the number of C_1 and C_2 in ethylene decomposition products was the largest while the number of oxygen molecules was 60, which further indicated that the highly reactive oxygen groups provided by oxygen aggravate the fracture of carbon-carbon bonds in ethylene.

3.3.2. Chemical bonds and and key species evolution behavior

To further investigate the reasons for the differences in ethylene decomposition products induced by oxygen. Fig. 10 showed the changes in the number of chemical bonds during the oxygen induced ethylene decomposition evolution process. Comparing the changes in chemical bonds between systems with oxygen concentrations of 20 and 60, as shown in Fig. 10 (a) and (b), respectively, and disregarding the variations in oxygen–oxygen single and double bonds due to oxygen concentration, significant differences were observed in the behavior of carbon–carbon single bonds. In the initial stage of the ethylene reaction, the carbon–carbon double bonds first dissociated into carbon–carbon single bonds. In low oxygen concentration, the number of carbon–carbon single bonds continued to increase even after the double bond reached its minimum. At this stage, the increase in carbon–carbon single bonds was primarily attributed to the polymerization reaction between ethylene radicals. In contrast, in high oxygen concentration, the number of carbon–carbon single bonds initially increased and then decreased, suggesting that ethylene formed active intermediates with oxygen free radicals after the double bonds were broken. The dissociation energy of the carbon–carbon bonds in this active intermediate was low, effectively facilitating the decomposition of ethylene.

By extracting key intermediate products during the ethylene decomposition process, the decomposition pathway of ethylene was further analyzed. The variation curves and differences of key products were presented in Fig. 11. In Fig. 11 (a), the production of CO was associated with a decrease in the quantities of C_2HO and C_2H_2O radicals. Around 50 ps, the concentration of CO began to increase, corresponding to a decrease in the number of C_2H_2O. On one hand, C_2H_2O underwent C—C bond broken to produce CO, and on the other hand, C_2H_2O underwent a dehydrogenation reaction to form C_2HO. Subsequently, C_2H_2O underwent further C—C bond broken to generate CO. The differences in the variation of key intermediate products with oxygen concentration, as shown in Fig. 11 (b), indicated that played a promoting role in ethylene decomposition. This to some extent highlighted the mechanistic influence of key intermediates in driving the shift of ethylene reactivity from polymerization-dominated processes toward decomposition-dominated pathways. The oxygen change the identity of the initial/final states and enable O-assisted activation channels (*i.e.*, σ-bond metathesis/oxidative-addition with reductive-deprotonation or proton-coupled electron transfer), thereby lowering transition-state energies compared with direct cleavage routes [32–34]. At low oxygen concentrations, oxygen mainly reacted with ethylene to produce C_2H_3 free radicals to initiate the reaction. As the oxygen concentration increases, however, abundant oxygen-centered radicals were generated, which significantly accelerated chain reactions and shifted the mechanism from polymerization-induced decomposition toward oxidative pyrolysis.

3.3.3. Major product reaction pathways

The proportion of reaction pathways for key products is shown in Fig. 12. CO was generated by the decomposition of groups containing carbonyl C—O, *e.g.*, CHO → CO + H, CHO_2 → OH + CO, among which CHO → CO + H was the most important reaction path. In addition, it could be directly decomposed into two CO through the cleavage of the C–C bond of the C_2O_2. During the simulation process, the gas produced by the reaction cannot be released in a timely manner. Since CO is generated in the early stage of the reaction, it readily combines with a large amount of free H and itself within the system, leading to a higher frequency of

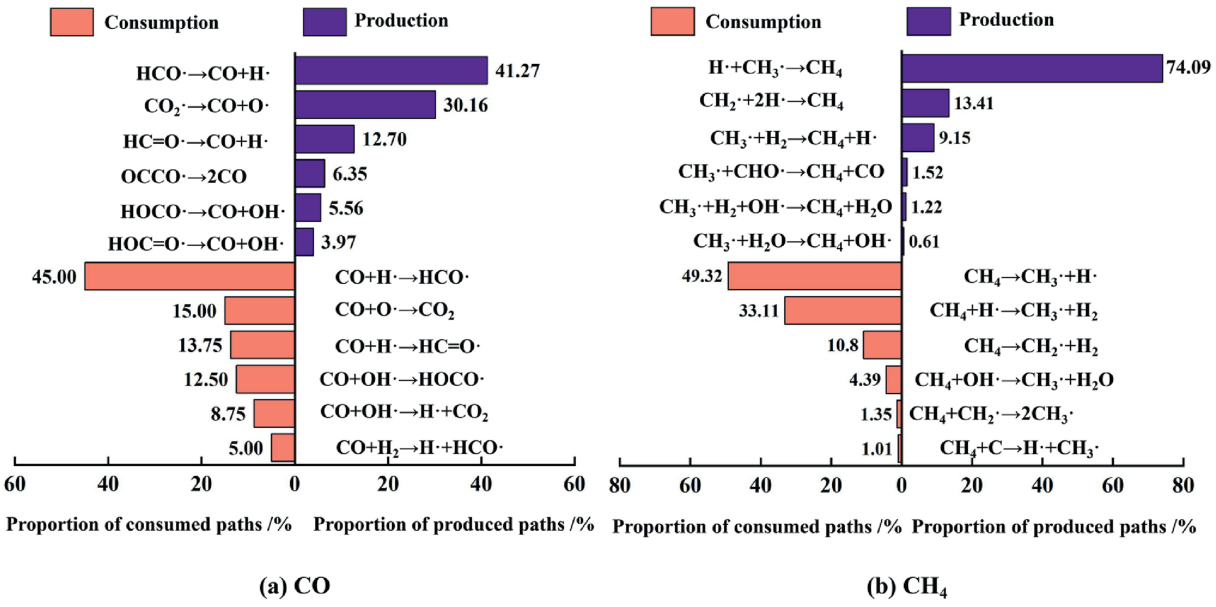

Fig. 12. Proportion of formation and consumption reactions of key reactants and products.

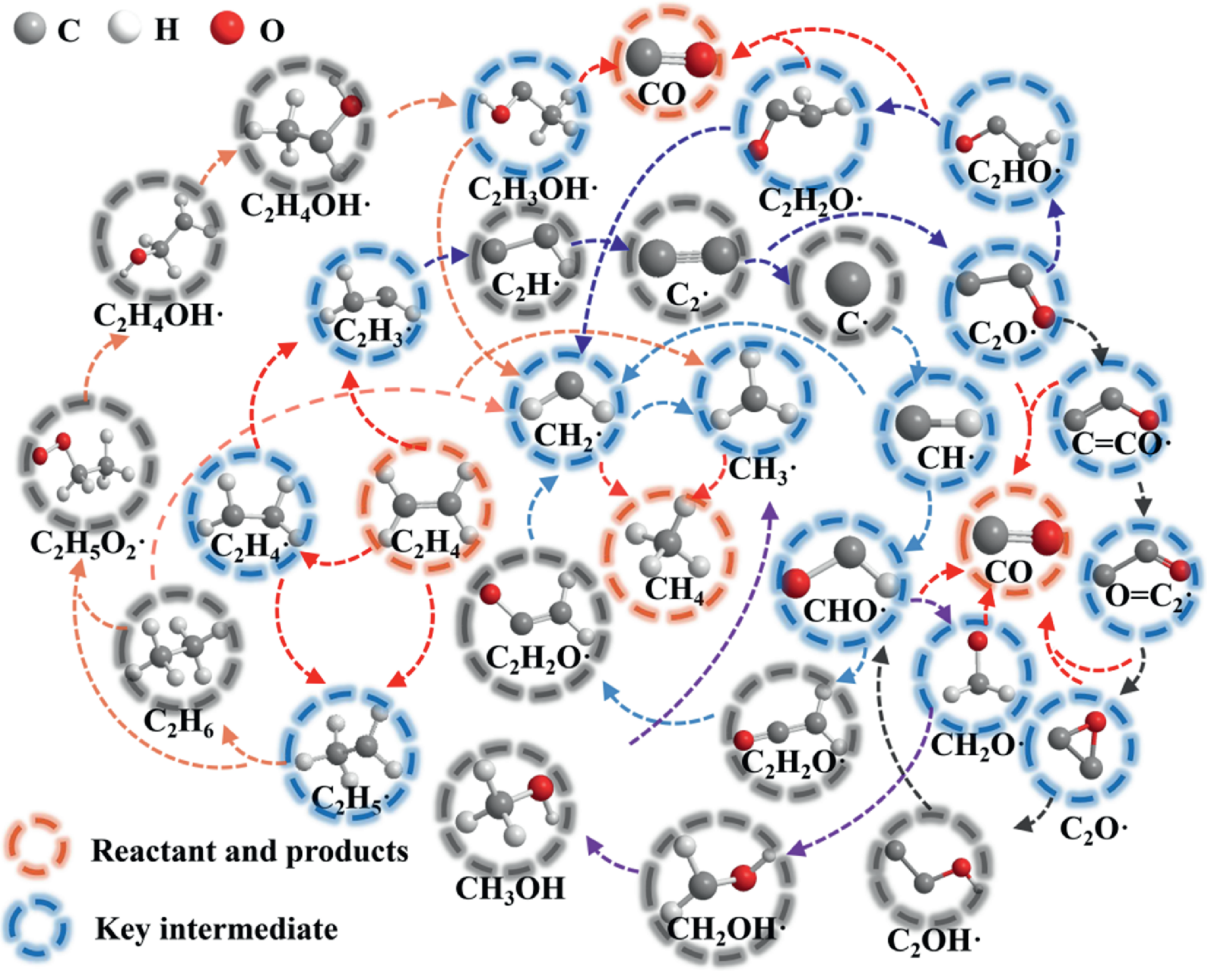

Fig. 13. Ethylene decomposition reaction transformation pathways.

such reactions. As expected, most of the CH_4 molecules were generated from the additive reaction of CH_3 and CH_2, *e.g.*, $CH_3 + H \rightarrow CH_4$, $CH_2 + 2H \rightarrow CH_4$, whose inverse reaction was also the main consumption pathway. By constructing the reaction network, the specific pathway of oxygen induced ethylene decomposition reaction would be revealed.

The ethylene decomposition reaction network was shown in Fig. 13. Ethylene initially broke the carbon-carbon double bond and underwent dehydrogenation. While the two carbon atoms in ethylene became saturated or lack hydrogen atoms, the carbon-carbon bond was more likely to break. Due to the high bond dissociation energy of the carbon-carbon bond, a significant amount of energy was required, and multiple intermediates were traversed for it to break. The bond dissociation energy of the carbon-oxygen bond in the oxygen-containing intermediate was lower than that of the carbon-carbon bond, making the oxygen-containing intermediate more likely to break the carbon-carbon bond and promote more thorough ethylene decomposition, facilitating the generation of CH_4. In addition, compared to produce CH_4, oxygen-containing groups needed undergo multi-step reactions, while fewer reactions were required to generate CO. This resulted in a significantly higher CO content compared to CH_4 in the simulation results. The oxygen content in the experiment was minimal. Once the chain reaction of ethylene decomposition was successfully initiated by oxygen, anaerobic decomposition became dominant, resulting in a high CH_4 content in the experimental results.

4. Conclusions

This study focused on the impact of oxygen on the decomposition and evolution mechanism of ethylene, the decomposition mechanism of ethylene was revealed, the evolution law of oxygen-induced supercritical ethylene decomposition was clarified, and the reaction network of supercritical ethylene decomposition was constructed. The results indicated that at 240 °C and 240 MPa, an oxygen concentration of 0.0042% could initiate the decomposition of supercritical ethylene, leading to a maximum pressure of 532 MPa and a maximum temperature of 553 °C. The increase in oxygen concentration has shortened the time required for the decomposition of supercritical ethylene from 14 s to 2 s. The main products of ethylene decomposition were methane, hydrogen, and spherical solid carbon. Oxygen and the oxygen atoms generated from its decomposition exist in a triplet state, providing active sites for subsequent reactions with ethylene. These species readily interacted with ethylene to form unstable intermediates such as $C_2H_xO\cdot$, which promoted the breaking of C—C bond and thereby intensified ethylene decomposition. In contrast, under oxygen-free conditions, ethylene predominantly underwent polymerization reactions accompanied by carbon-chain growth. This study provided data support and the theoretical basis for ensuring the safe and stable production of low density polyethylene.

The supercritical ethylene decomposition process was extremely complex, and the underlying mechanism of ethylene decomposition required further description and investigation. The

accuracy of ReaxFF molecular dynamics simulation was affected by the reaction force field. To conduct more precise and detailed mechanism research, force field training should be conducted on the system of supercritical ethylene.

CRediT Authorship Contribution Statement

Yao Chen: Writing – original draft, Methodology, Data curation. Zhichen Zhang: Writing – original draft. Yunfeng Zhu: Writing – review & editing. Haowen Chen: Writing – review & editing. Yifan Song: Writing – review & editing. Ruiyi Zhang: Writing – review & editing. Xiaogang Shi: Writing – review & editing. Bing Sun: Writing – review & editing, Funding acquisition. Wei Xu: Writing – review & editing, Funding acquisition.

Declaration of Competing Interest

We declare that we have no financial and personal relationships with other people or organizations that can inappropriately influence our work.

Acknowledgements

The authors gratefully acknowledge financial support from the National Key Research and Development Program of China (2024YFC3082600), and the National Natural Science Foundation of China (22278452, 22378437).

References

[1] Y. Gao, Y. Yao, H. Li, J. Dong, Review and prospect of polyethylene market development at home and abroad, *Sino-Global Energy* 27 (2022) 58–63. (in Chinese)
[2] H.J. Lee, Y.K. Yeo, J.Y. Changn, Modeling of industrial high pressure autoclave polyethylene reactor including decomposition phenomena, *Kor. J. Chem. Eng.* 17 (2) (2000) 223–229.
[3] Z.C. Zhang, W. Xu, Y.F. Zhu, S.T. Ma, Y.H. Li, J. Jiang, Z. Yang, W.S. Cheng, Z.C. Zhou, B. Sun, The decomposition mechanism of ethylene and modeling simulation during LDPE production: a comprehensive review and perspectives, *J. Anal. Appl. Pyrolysis* 175 (2023) 106199.
[4] Y.C. Cheng, S.C. Chang, C.M. Shu, Effects of volatile organic compounds on the explosion characteristics of polyethylene dust, *Process Saf. Environ. Prot.* 168 (2022) 114–122.
[5] G. Luft, R. Neumann, Selbstzerfall und fremdgezündeter zerfall von verdichtetem äthylen, *Chem. Ing. Tech.* 50 (8) (1978) 620–622.
[6] D.I. Shannon, Relief device sizing for ethylene decompositions: high pressure polyethylene industry, *Process Saf. Prog.* 27 (1) (2008) 35–40.
[7] O. Ashrafi, N. Mostoufi, R. Sotudeh-Gharebagh, Two phase steady-state particle size distribution in a gas-phase fluidized bed ethylene polymerization reactor, *Chem. Eng. Sci.* 73 (2012) 1–7.
[8] S.X. Zhang, N.K. Read, W.H. Ray, Runaway phenomena in low-density polyethylene autoclave reactors, *AIChE J.* 42 (10) (1996) 2911–2925.
[9] Y. Fei, B. Sun, F. Zhang, W. Xu, N. Shi, J. Jiang, Inherently safer reactors and procedures to prevent reaction runaway, *Chin. J. Chem. Eng.* 26 (6) (2018) 1252–1263.
[10] Y.N. Yang, J. Jin, L.T. Zhu, Y.N. Zhou, Z.H. Luo, Runaway criteria for predicting the thermal behavior of chemical reactors, *Curr. Opin. Chem. Eng.* 43 (2024) 100986.
[11] X.Q. Fan, J.Y. Sun, J.D. Wang, Z.L. Huang, Z.W. Liao, G.D. Han, Y.R. Yang, Scale-up and thermal stability analysis of fluidized bed reactors for ethylene polymerization, *Chin. J. Chem. Eng.* 62 (2023) 281–290.
[12] J. Albert, G. Luft, Runaway phenomena in the ethylene/vinylacetate copolymerization under high pressure, *Chem. Eng. Process. Process. Intensif.* 37 (1) (1998) 55–59.
[13] J.C. Wang, Cause analysis and countermeasures of ethylene decomposition in high pressure polyethylene plant, *Knowl. Econ.* 15 (2013) 72–73. (in Chinese)
[14] N.H. Kolhapure, R.O. Fox, A. Daiβ, F.O. Mähling, PDF simulations of ethylene decomposition in tubular LDPE reactors, *AIChE. J.* 51 (2) (2005) 585–606.
[15] L. Bao, Cause analysis and control measures for decomposition reactions in LDPE plant, *Sino-Global Energy* 25 (2020) 79–82. (in Chinese)
[16] M.X. Zhou, F.W. Yan, X.L. Zhong, L. Xu, Y. Wang, Sooting characteristics of partially-premixed flames of ethanol and ethylene mixtures: unravelling the opposing effects of ethanol addition on soot formation in non-premixed and premixed flames, *Fuel* 291 (2021) 120089.
[17] L. Song, C.C. Xu, J. Ye, Y. Zhang, B. Chen, F.C. Hou, B.C. Chen, H.L. Su, J. Sun, Pyrolysis and oxidation mechanisms of ethylene and ethanol blended fuel based on ReaxFF molecular dynamics simulation, *Fuel* 373 (2024) 132361.
[18] J.H. Martin, B. Akih-Kumgeh, Reactive molecular dynamics simulation of methane-oxygen autoignition at high-pressure conditions, *Int. J. Chem. Kinet.* 57 (11) (2025) 662–673.
[19] Z.J. Chen, W.Z. Sun, L. Zhao, High-temperature and high-pressure pyrolysis of hexadecane: molecular dynamic simulation based on reactive force field (ReaxFF), *J. Phys. Chem. A* 121 (10) (2017) 2069–2078.
[20] B. Wang, C.C. Wang, B.L. Lv, Comparative analysis on safety of polyethylene production process by high pressure method and low pressure method, *Ind. Des.* 9 (2011) 156.
[21] K. Yamada, S. Kumagai, T. Shiratori, T. Kameda, Y. Saito, A. Watanabe, C. Watanabe, N. Teramae, T. Yoshioka, Combined UV-irradiation and pyrolysis-GC/MS approach for evaluating the deterioration behavior of ethylene vinyl acetate, *Polym. Degrad. Stab.* 190 (2021) 109623.
[22] Y. Chen, Z.C. Zhang, Y.F. Zhu, X.G. Shi, B. Sun, W. Xu, Research on the explosion behavior and flame evolution characteristics of LDPE powder with different sizes, *Process. Saf. Environ. Prot.* 195 (2025) 106735.
[23] C.A. Gunawardana, A. Kong, D.O. Blackwood, C. Travis Powell, J.F. Krzyzaniak, M.C. Thomas, C. Calvin Sun, Magnesium stearate surface coverage on tablets and drug crystals: insights from SEM-EDS elemental mapping, *Int. J. Pharm.* 630 (2023) 122422.
[24] Z.C. Zhang, E.Q. Yu, Y.J. Liu, F.S. Wen, N. Shi, H. Du, Z.J. Chen, Z.C. Wang, D. Liu, The effect of composition change and allocation in raw material on the carbonaceous structural evolution during calcination process, *Fuel* 309 (2022) 122173.
[25] S. Na, H. Jeong, I. Kim, S.M. Hong, J. Shim, I.H. Yoon, K.H. Cho, Distribution coefficient prediction using multimodal machine learning based on soil adsorption factors, XRF, and XRD spectrum data, *J. Hazard. Mater.* 478 (2024) 135285.
[26] Z.C. Zhang, Y. Chen, Y.F. Zhu, Y.H. Li, S.T. Ma, H.W. Chen, Z.Q. He, H.C. Bao, J. Jiang, B. Sun, W. Xu, Decomposition behavior of supercritical ethylene under ultra-high temperature and ultra-high pressure, *J. Anal. Appl. Pyrolysis* 181 (2024) 106654.
[27] Y. Chen, Z.C. Zhang, Y.F. Zhu, Y.H. Li, S.T. Ma, H.W. Chen, J. Jiang, B. Sun, W. Xu, Investigation on the effect of carbon powder structural characteristics derived from ethylene decomposition on powder explosion, *Thermochim. Acta* 742 (2024) 179895.
[28] Z.C. Zhang, Z.H. Wang, L.J. Zhang, J.J. Cui, S.H. Guo, H.H. Ji, Y.J. Liu, G.L. Zhao, W. Zhu, C. Jiao, Y.G. Cao, D. Liu, Study on the co-carbonization behavior of high-temperature coal tar pitch and raffinate oil of low-temperature coal tar, *Fuel* 310 (2022) 122469.
[29] Y.B. Wang, S.J. Yao, W. Wang, C.L. Qiu, J. Zhang, S.W. Deng, H. Dong, C. Wu, J. G. Wang, Pyrolysis of vulcanized styrene-butadiene rubber *via* ReaxFF molecular dynamics simulation, *Chin. J. Chem. Eng.* 31 (2021) 94–102.
[30] J.T. Cai, Q.F. Huang, H. Chen, T. Zhang, B. Niu, Y.Y. Zhang, D.H. Long, Evaluating two stages of silicone-containing arylene resin oxidation *via* experiment and molecular simulation, *Chin. J. Chem. Eng.* 66 (2024) 189–202.
[31] C. Ashraf, A.C.T. van Duin, Extension of the ReaxFF combustion force field toward syngas combustion and initial oxidation kinetics, *J. Phys. Chem. A* 121 (5) (2017) 1051–1068.
[32] D. Hibbitts, M. Neurock, Promotional effects of chemisorbed oxygen and hydroxide in the activation of C–H and O–H bonds over transition metal surfaces, *Surf. Sci.* 650 (2016) 210–220.
[33] B. Xing, G.C. Wang, Insight into the general rule for the activation of the X-H bonds (X = C, N, O, S) induced by chemisorbed oxygen atoms, *Phys. Chem. Chem. Phys.* 16 (6) (2014) 2621–2629.
[34] B. Xing, X.Y. Pang, G.C. Wang, C–H bond activation of methane on clean and oxygen pre-covered metals: a systematic theoretical study, *J. Catal.* 282 (1) (2011) 74–82.